Available online at www.sciencedirect.com
SCIENCE DIRECT®
Journal of Electroanalytical Chemistry 568 (2004) 273–291
Journal of Electroanalytical Chemistry
www.elsevier.com/locate/jelechem

# Oxygen reduction and transport characteristics at a platinum and alternative proton conducting membrane interface

Lei Zhang, Chengsong Ma, Sanjeev Mukerjee *

*Department of Chemistry, Northeastern University, 360 Huntington Avenue, Boston, MA 02115, USA*

Received 13 January 2004; accepted 8 February 2004
Available online 11 March 2004

**Abstract**

Kinetic and mass-transport properties were investigated for the oxygen reduction reaction for Nafion® 117 and sulfonated poly(arylene ether sulfone) membranes, both pre- and post-sulfonated analogs (SPES-40 & SPES-PS) under 100% relative humidity and as a function of pressure (1–4 atm total pressure, 323 K) and temperature (303–353 K, 3 atm) using a solid-state electrochemical cell. Kinetic parameters were obtained using slow-sweep voltammetry while mass-transport parameters, the diffusion coefficient ($D$) and solubility ($C$), were obtained using chronoamperometry at a Pt (microelectrode)|proton exchange membrane (PEM) interface. The oxygen reduction kinetics were found to be similar for all the membranes at the Pt microelectrode interface. The temperature dependence of $O_2$ permeation parameters showed identical trends for the membranes studied while the pressure dependence of $O_2$ permeation parameters displayed some differences. Despite higher ion exchange capacities and hence higher water uptake, the two SPES membranes exhibited relatively lower values of $D$ as compared to Nafion® 117. The results are discussed in the context of their different microstructures.


*Keywords:* Sulfonated poly(arylene ether sulfone); Oxygen diffusion coefficient; Oxygen solubility; Oxygen permeability; Microelectrode

## 1. Introduction

Proton exchange membrane fuel cells (PEMFCs) are candidate power sources for vehicular transportation, residential and consumer electronics [1]. Amongst the key components is the polymer electrolyte membrane (PEM) that provides the ionic pathway and acts as a gas separator. The current state-of-the-art is based on perfluorinated sulfonic acid chemistry, such as those from Dupont (Nafion®), Asahi chemicals (Aciplex®) and others. These membranes achieve good performance when operating at 80–90 °C and high relative humidity (>80% RH) [2–4]. They have good mechanical strength, chemical stability (up to 60,000 h of operation at 80 °C) and high proton conductivity [1]. However, these membranes remain expensive and have several limiting factors such as low conductivity at low relative humidity [5], high methanol permeability [6,7], and a low $T_g$ (glass transition temperature) [8] which restricts its application to below 100 °C.

Transitioning to temperatures above 100 °C provides for several attractive options which include higher CO tolerance [9,10], better water and heat management related to interfacing fuel cells with other system components such as the fuel processor unit.

Alternative hydrated membranes to the perfluorinated sulfonic acid based systems possessing high proton conductivity at lower relative humidity and stability at elevated temperatures are currently the focus of much research and development. Most of them are based on engineering polymers with high thermo-chemical stability [11], typically with a high degree of aromatic character, where the monomer consists of a variety of fused phenyl rings linked together with a number of bridging moieties (referred herein as membranes with aromatic backbones). Sulfonation of these materials involves either using a sulfonated monomer in the polymer synthesis or using a variety of methods for

* Corresponding author. Tel: +1-617-373-2382; fax: +1-617-373-8949.
*E-mail address:* smukerje@lynx.neu.edu (S. Mukerjee).

0022-0728/$ - see front matter © 2004 Published by Elsevier B.V.
doi:10.1016/j.jelechem.2004.02.003

post-sulfonation. Several families of polymers have been developed in this context; these include sulfonated polyether (ether) ketone (SPEEK) [12], polyimides [13], polyether sulfone (SPES) [14,15], polysulfide sulfone (SPSS) [16,17], polyphenyl quinoxaline (SPQQ) [18], aryl oxyphosphazene (SAOP) [19], propylated poly(benzimidazole) [20–22] and poly(phenylene sulfide sulfone) [23].

In this search for elevated-temperature PEMs, the sulfonated poly(arylene ether sulfone) (SPES) family has recently been reported as a promising candidate material [24–28]. Being well-known engineering thermoplastics, poly(arylene ether sulfones) (Structure 1) display a high glass transition temperature ($T_g$) of 195 °C, good resistance to hydrolysis and oxidation, excellent mechanical properties and high thermal stability [29]. The closely related poly ether sulfone (Structure 2) is totally devoid of aliphatic hydrocarbon groups and exhibits even higher thermal stability ($T_g = 230$ °C) [30]. Sulfonation of the poly(arylene ether sulfone) for application as a practical proton exchange membrane for fuel cells is therefore motivated on the basis of its potential capability for elevated temperature operation. A commonly used method for synthesizing SPES is attaching sulfonic acid groups by polymer modification reactions (post-sulfonation route). Foster-Miller Inc. (Waltham, MA), for example, synthesized their membranes by post-sulfonation of commercially available poly(phenylene ether sulfone) material (commercially referred to as Radel® R), referred to herein as SPES-PS [31]. Recently, direct polymerization of SPES using sulfonated monomers was reported by Wang et al. [32] of the Virginia Polytechnic Institute and State University (Virginia Tech.). The polymer synthesized at Virginia Tech., (commonly referred to by the Virginia Tech. group as PBPSH-XX) contains copolymers with high sulfonation levels (XX = 40–60, where XX represents the fraction of the sulfonated component in these copolymers), each sulfonated component containing two sulfonate groups per repeat unit. These polymers have shown proton conductivity in excess of 0.08 S cm$^{-1}$ (at room temperature), which meets the requirement for high-performance PEMFC [32].

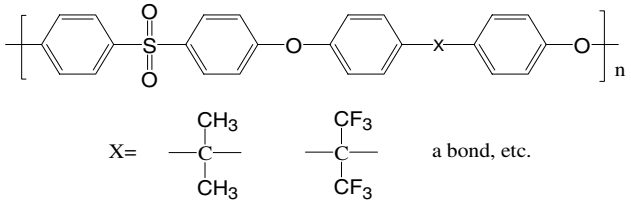


Structure 1. Poly(arylene ether sulfones).

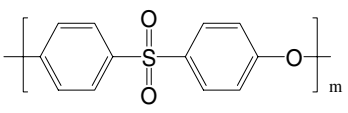


Structure 2. Polyether sulfone.

These membranes however represent very different chemistry relative to the conventional perfluorosulfonate systems such as Nafion®. In addition to the very distinct backbone structure, usually greater ion exchange capacities (IEC) are needed with these sulfonated poly(arylene ether) polymers to obtain comparable ion exchange conductivities as Nafion®, since the acidity of the pendent perfluorosulfonic acid of the perfluorosulfonate polymer is much stronger than the aryl sulfonic acid [32]. The use of these new materials as ion conducting components in PEM fuel cells operating at elevated temperatures not only requires excellent proton conduction, preferably at low relative humidity (RH), but also compatible (relative to perfluorinated systems) reactant transport characteristics. For an electrochemical charge transfer to be successful only the dissolved reactant moieties are relevant, therefore efficient transport of reactant species such as oxygen within the electrolyte is crucial. This efficient reactant transport or permeation comprises of two important components, the solubility ($C$), and diffusion coefficient ($D$). Together, they determine the crossover of gases across the membrane thus affecting the open circuit potential. More importantly, they determine the availability of the reactant at the electrocatalyst|electrolyte interface. This is most important in determining the onset of mass transport limitations in a typical fuel cell performance.

In previous publications, mass-transport parameters for oxygen reduction reaction at the interface between Pt and a variety of solid-state perfluorosulfonic acid-type materials (Nafion® and Aciplex® membranes) have been studied intensively since the pioneering work of Parthasarathy et al. [33]. Prior studies on oxygen transport characteristics in these membranes have examined the effect of both environmental (temperature and pressure) [34–36] and membrane structural composition (equivalent weight) [37]. Similar investigations had been made on a series of sulfonated α, β, β-trifluorostyrene (BAM®, Ballard, Canada) membranes and sulfonated styrene–(ethylene–butylene)–styrene triblock copolymers (DAIS®, DAIS-Analytic, USA) by Holdcroft and coworkers [36,38,39]. These studies suggested that oxygen transport behavior was primarily related to water content in the membranes. The effect of an increase in equivalent weight [39] was shown to cause a decrease in diffusion coefficient of oxygen and increase in the solubility.

We have recently reported oxygen permeation characteristics and interfacial kinetics at a SPES-40 (40% sulfonated poly(arylene ether sulfone)) and Nafion® 117 membrane/microelectrode interface measured at ambient pressure conditions [40]. In this previous report,

SPES-40 and Nafion® 117 were found to have relatively close diffusion coefficients, despite the higher water uptake by SPES-40 (approximately twice the IEC). The oxygen solubility for Nafion® 117 was however significantly higher than SPES-40. These results were discussed in the context of water content and microstructure of the membranes. The conformations of water-filled channels connecting the hydrophilic ionic clusters appear to make important contributions in the process of $O_2$ diffusion. The chemistry of the SPES membrane backbone appears to play a major role in determining the solubility of oxygen in these systems, given its relatively lower hydrophobicity as compared to the perfluorinated aliphatic backbone of Nafion®. From an overall perspective, the lower solubility of oxygen in the SPES membrane appears to effect the overall permeation of oxygen in this class of membranes.

The effects of pressure on both the diffusion coefficient and solubility of oxygen in perfluorinated aliphatic proton exchange membranes have been studied previously [35,36]. Parthasarathy et al. [35] reported no variation of diffusion coefficient of oxygen in perfluorinated sulfonic acids (Nafion®) as a function of pressure. In this prior report however, the air equilibrated membranes exhibited lower diffusion coefficients as compared to the $O_2$ equilibrated samples. The possibility of $N_2$ enabling longer diffusion – pathways in the membrane was advanced. Later Holdcroft and coworkers [36], reported variations of diffusion coefficients with pressure for Nafion® 117; an increase in the diffusion coefficient by 35% was reported in the pressure range of 2–5 atm ($O_2$). A similar variation (~25%) was also reported for a membrane based on sulfonated trifluorostyrene copolymers (Ballard Advanced Membrane, BAM®, Ballard, Canada) in the same pressure range. Very few data however exist on the variation of diffusion coefficient between ambient and 1 atm total pressure. Both the prior reports by Parthasarathy et al. [35] and Holdcroft and coworkers [36] have reported a linear dependence of oxygen solubility with pressure in accordance with Henry's law. Parthasarathy et al. [35] reported different Henry constants in air and oxygen equilibrated samples for Nafion®, the air equilibrated sample exhibiting a higher value. The corresponding Henry's law constants reported by Holdcroft [36] were slightly higher for Nafion®, however more interestingly their data on BAM® membranes (EW = 407) were three fold higher as compared to the corresponding data for Nafion®.

In this investigation our aim is to evaluate SPES membranes as candidate electrolytes for PEMFCs by investigating their oxygen transport and interfacial kinetics under conditions that mimic the practical operating conditions of a PEM fuel cell. The effects of temperature and pressure on the ORR kinetics and mass transport at a Pt microelectrode|membrane interface were investigated. The parameters obtained are compared with corresponding values for a Nafion® 117 membrane (control experiment). More importantly, the changes in the oxygen transport characteristics were studied in the context of the very different chemistries of these polymer membranes, especially in lieu of the different nature of the phase segregation (hydrophobic and sulfonated hydrophilic components) in these new alternative membranes relative to those based on perfluorinated sulfonic acid (Nafion® analogs).

## 2. Experimental

### 2.1. Membranes

Three membranes were studied in this investigation. The first, sulfonated poly(arylene ether sulfone) (Structure 3), containing two sulfonate groups per repeat unit was prepared by Virginia Polytechnic and State University. The copolymer, PBPSH-40 ($100n/n+m=40$) [Virginia Tech., acronym] is referred to as SPES-40 in this paper. Detailed preparation methodology, reaction conditions and membrane properties, such as $T_g$, hydrophilicity, viscosity, TGA, AFM (hydrophilic domain size, phase inversion) and proton conductivity are reported elsewhere [32]. The second, sulfonated poly(arylene ether sulfone) post-sulfonated membrane (Structure 4 [41], referred to as SPES-PS) was developed by Foster-Miller, Inc. (Waltham, MA) [31]. The third, Nafion® 117 (Structure 5) was bought from Aldrich Chemicals; this served as a control based on the wealth of prior data regarding both interfacial kinetics and $O_2$ transport parameters.

All membranes were soaked in 1 M sulfuric acid for 48 h at room temperature to ensure full protonation. After protonation, the membranes were rinsed several times and stored in de-ionized water.

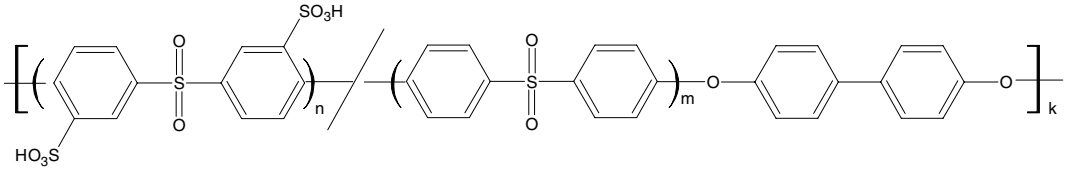


Structure 3. Sulfonated polyarylene ether sulfone (SPES-40).

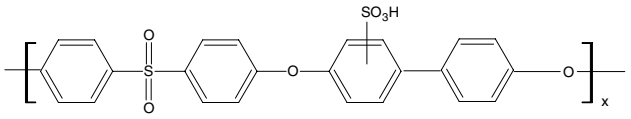

Structure 4. Sulfonated polyarylene ether sulfone-post-sulfonated (SPES-PS).

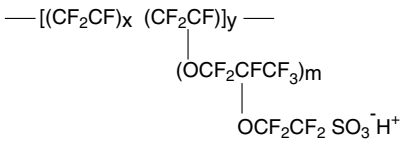

Structure 5. Nafion® 117.

Measurements of water uptake followed typical methods reported earlier [39]. Membranes were initially dried at 80 °C in a vacuum oven, overnight (12 h). The membranes were equilibrated by immersing them in an enclosed water container, which was placed in a constant temperature oven. Following equilibration for 4–6 h at the desired temperature, the membranes were quickly weighed, taking care that excess water was removed prior to weighing. This allowed measurement of water uptake as a function of temperature. The water content in terms of wt% was determined according to: $H_2O$ [%] = [(wet weight − dry weight)/dry weight] × 100%. The number of moles of water per sulfonic acid group ($\lambda = [H_2O]/SO_3^-$) was also calculated.

### 2.2. Electrodes

The working electrode was a 100 μm diameter Pt microelectrode (Bioanalytical Systems Inc., West Lafayette, IN). The surface of the microelectrode was polished with 5, 3 and 1 μm diamond solution and finally with 0.05 μm alumina polish (BAS-polishing kit). Following the polishing step, the electrode was sonicated in deionized water for 60 s and rinsed. It was stored in DI water before assembling in the electrochemical cell. A solid-state dynamic hydrogen electrode (DHE) served as the reference electrode. It was constructed by sealing two 0.25 mm diameter Pt wires (Alfa Aesar) in a double-bore glass tube. Prior to each experiment, the electrodes were platinized using a 20 mM chloroplatinic acid solution. A 9 V battery in series with a 2.2 MΩ resistor was used for a constant current supply between the two platinized electrodes in the DHE in contact with the hydrated membrane. The counter electrode was a 1.6 mm diameter Pt electrode (BAS) spot-welded to a 5 mm × 5 mm × 0.01 mm (thick) Pt foil.

### 2.3. Solid-state electrochemical cell setup

A cell setup was designed to perform solid-state electrochemical experiments under controlled pressure, temperature and relative humidity. A schematic of the cell is given in Fig. 1. The apparatus consisted of three Teflon blocks. The bottom Teflon block housed a glass base with a built-in fritted glass filter (47 mm diameter, Millipore), which had a porous and smooth flat surface to support the membrane of interest. The bottom end of the glass filter base was connected to the gas supply through a Swagelock® adapter, which had arrangements for sealed thermocouple and humidity sensor attachments. This enabled measurement of inlet gas temperature and humidity immediately below the membrane|electrode interface. The middle Teflon block had three through-holes to fit the working, counter and reference electrodes. This was used to provide conduits for the wires connecting these electrodes. The upper stainless steel block contained three flat-tip micrometer heads. By screwing forward its spindle, variable pressure could be applied to the electrode–membrane contact. Four screw rods and several nuts held the three blocks tightly together. A thermocouple (Omega Engineering, Stamford, CT) was inserted into the cell from the bottom with its tip touching the membrane. Temperature control was achieved by using a temperature controller (Watlow, series-965). During the experiment, the cell was put into a pressure container, capable of providing constant temperature and pressure, which also served as a Faraday cage. Gas was supplied using a special heating and humidity control unit. All results reported in this paper are at 100% relative humidity. The relative humidity was measured independently using a humidity sensor (ELECTRONIK, series EE-30) at the bottom of the solid-state microelectrode assembly. The flow rate of the humidified gas entering the cell was set at about 600 ml $min^{-1}$.

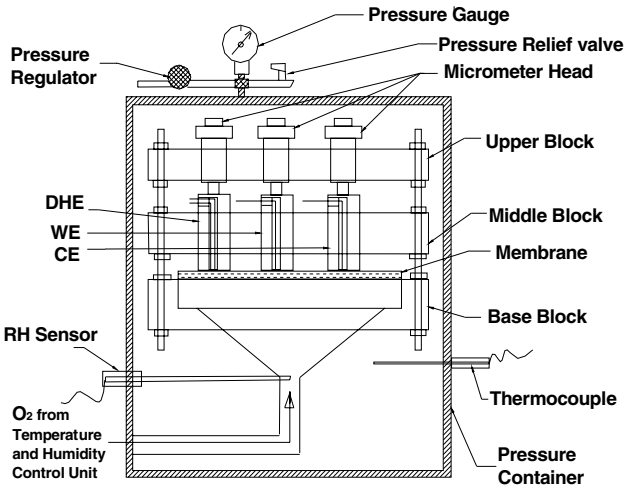


Fig. 1. Schematic of the solid-state microelectrode set up with arrangements for performing experiments under controlled temperature and pressure conditions.

The overall set up of this electrochemical cell was based on earlier designs [33–35]. In our set up all the

electrodes were on the same side of the membrane, instead of having the membrane sandwiched between the working electrode on one side and the counter and reference electrodes on the other. The modification in our set up ensured good mechanical contact at the membrane|electrode interface. This was achieved using micrometer heads, which could be more conveniently used to adjust the clamping pressure as compared to springs in previous cell setups [33–35]. In this arrangement the distance between the working and the reference electrode was similar to those in previous setups [33]. The impedance between working and reference electrodes was monitored and standard iR correction methods applied (Echochemie, model AUTOLAB PGSTAT 30).

### 2.4. Electrochemical techniques and instrumentation

A computer controlled digital potentiostat/galvanostat (Autolab model, PGSTAT-30) was employed to conduct cyclic voltammetry, slow-sweep voltammetry and chronoamperometry experiments. All potentials stated here are relative to DHE.

Cyclic voltammetry (scan rate = 50 mV $s^{-1}$) in the potential range 0.08–1.5 V in nitrogen was carried out to evaluate the electrochemically active area and roughness factors of the Pt microelectrode. Fast scan cyclic voltammetry (0.08–1.5 V) in oxygen at a scan rate of 100 mV $s^{-1}$ was performed during the equilibrium periods at each temperature for cleaning and activating the Pt microworking electrode.

Slow-sweep voltammograms were recorded in the potential range, 1.2–0.3 V, with a scan rate of 2 mV $s^{-1}$ to determine the limiting current $I_d$, which is given by equation (1):

$$I_d = n\pi FDCr, \tag{1}$$

where $n = 4$, referring to the number of electrons transferred per mole of oxygen in the overall $O_2$ reduction at Pt electrode ($O_2 + 4e^- + 4H^+ \rightarrow 2H_2O$), $F$ is Faraday's constant, $D$ is the diffusion coefficient of $O_2$, $C$ is the solubility of $O_2$ and $r$ is the radius of the Pt microelectrode. Electrode kinetic parameters were obtained using slow scan voltammograms. For this the mass-transport corrected Tafel equation was used:

$$\eta = \frac{2.303RT}{\alpha nF}\log i_0 + \frac{-2.303RT}{\alpha nF}\log\left[\frac{i_d i}{i_d - i}\right], \tag{2}$$

where, $\eta$ is the overpotential ($E - E^0$), $R$ is the gas constant, $T$ is the absolute temperature, $\alpha$ is the transfer coefficient, $n$ is the number of electrons involved in the rate determining step of $O_2$ reduction on Pt ($H_3O^+ + O_2 + e^- \rightarrow O_2H_{(ads)} + H_2O$), $i_0$ is the exchange current density, $i_d$ is the limiting current density, and $i$ is the current density. The activation energy for oxygen reduction reaction was obtained from Arrhenius plots based on the following equation:

$$E_a = -2.303R\left[\frac{d\log i_0}{d(1/T)}\right]. \tag{3}$$

A chronoamperometry experiment was used to determine the diffusion coefficient and solubility of oxygen. It was performed by holding the potential of the microelectrode at 1.2 V for 20 s and then stepping to 0.4 V, and holding for 5 s. A plot of current, $I$, vs. reciprocal of the square root of time, $t^{-1/2}$, for a time domain from 1 to 5 s gave a linear relationship corresponding to the modified Cottrell equation given below

$$I(t) = \frac{nFAD^{1/2}C}{\pi^{1/2}t^{1/2}} + \pi FnDCr, \tag{4}$$

where $A$ is the geometric area of the microelectrode. $D$ and $C$ values were obtained simultaneously from linear regression analysis of the slope and intercept. For details on the choice of this equation and use of this methodology see [33–36]. The activation energy of $O_2$ diffusion and enthalpy of dissolution of $O_2$ in the membranes were calculated according to the following equations given below:

$$E_d = -2.303R\left[\frac{d\log D}{d(1/T)}\right], \tag{5}$$

$$\Delta H_s = -2.303R\left[\frac{d\log C}{d(1/T)}\right]. \tag{6}$$

### 2.5. Experimental procedure

After incorporation into the cell, the membrane was equilibrated with humidified gas at 303 K and ambient pressure for at least 12 h. The temperature dependence studies of oxygen reduction and transport measurements were conducted at 100% relative humidity in a temperature range of 303–353 K and 3 atm pressure ($O_2$, total pressure). The pressure dependence studies of oxygen reduction and transport characteristics were conducted at 323 K, 100% RH in a pressure range of 1–4 atm ($O_2$, total pressure) or air 1.5–3.5 atm (air, total pressure, corresponding partial pressure of oxygen ≈0.3–0.7 atm). Series of electrochemical measurements were conducted to determine both interfacial kinetics and mass-transport parameters at each temperature and pressure condition after equilibration for at least 2 h. All experiments conducted for each of the membranes were repeated at least three times and the reproducibility monitored.

## 3. Result and discussion

### 3.1. Cyclic voltammogram at the Pt/PEM interface

Cyclic voltammetry (CV) was used to determine qualitatively the nature of the interfacial contact between

the Pt microelectrode and the hydrated membrane. The uncompensated resistance at the membrane electrode interface can shift the oxygen reduction wave to more negative potentials [33] which can constitute a source of error in the determination of the kinetic and mass-transport parameters. To minimize the effect of variability in contact resistance, the position of the micrometer heads were adjusted until the contact impedance stopped changing. The shift in the oxide reduction peak in CV was used as a convenient method to monitor the variability in the contact impedance. For this, the working electrode was exposed to an inert gas ($N_2$) under 100% RH conditions at a temperature of 303 K. The micrometer head which determines the contact pressure between the working electrode and electrolyte membrane was locked into position at the point where no further positive shift in the Pt oxide reduction peak was observed. Further, the impedance of the working electrode relative to the reference was monitored as a function of the micrometer head positions (contact pressure) until no further change was observed; this corresponded well with the shifts in the oxide reduction peak.

Well-resolved CVs obtained at the Pt microelectrode|PEM interface were used to evaluate the electrochemically active area and roughness factor of the microelectrode. Details of the calculations are reported elsewhere [42]. By averaging the area under the hydrogen adsorption and desorption waves and taking into account the double-layer charging area (assuming 210 $\mu C\ cm^{-2}$ for a smooth Pt surface [43]), the roughness factor of the microelectrode was determined and found to be in the range of 2–3. These values are in excellent agreement with previously reported roughness factors [34,36,44].

The microelectrode surface was cleaned and activated routinely during the periods of cell equilibration at each temperature using fast-scan CV (100 mV $s^{-1}$, in the potential range 0.08–1.5 V) under oxygen flow at 100% RH.

### *3.2. Evaluation of electrode kinetics of $O_2$ reduction at Pt/PEM interfaces by slow-scan voltammograms*

#### *3.2.1. Temperature dependence of the electrochemical reduction of $O_2$ at Pt/PEM interfaces*

Evaluation of the electrode kinetics of $O_2$ reduction at a Pt microelectrode|Nafion® 117 interface has been discussed in great detail elsewhere [34,36]. Briefly, slowly sweeping (2 mV $s^{-1}$) the potential of the working electrode at an $O_2$-equilibrated membrane gives rise to sigmoidal-shaped voltammograms. The diffusion-controlled regions of these pseudo-steady-state curves provide the magnitude of limiting current ($I_d$). The activation-controlled region is used to generate quantitative data for $O_2$ reduction kinetics via a mass-transport corrected Tafel analysis.

All potentials reported in this work are with respect to the DHE. It is well recognized that correction of this reference potential with respect to the standard hydrogen electrode (SHE) reference potential provides a more accurate picture of the absolute values of the exchange current densities. However, the reference potential for DHE shows variations as a function of temperature and pressure [45]. Hence using a correction term determined at one condition such as those reported earlier [36] (a correction of $-80 \pm 10$ mV, with respect to a calomel electrode measured in 0.5 M $H_2SO_4$ at room temperature), is not expected to hold over the entire temperature range [45]. Since the purpose here is to compare the kinetics of the orr at a Pt microelectrode|membrane interface, shifts from absolute values for exchange current densities were neglected. Comparison of all kinetic measurements with respect to the DHE provided a more stable and accurate comparison at different membrane interfaces.

Fig. 2 shows the representative slow-scan voltammograms for a Pt microelectrode/SPES-40 membrane at six different temperatures with 3 atm $O_2$ total pressure. The other two membranes studied gave similar responses. As expected, the oxygen reduction waves are shifted away from the theoretical reversible potentials $E_r$ due to poor reaction kinetics. The limiting current associated with the orr displays an increasing trend with temperature. Plots of $I_d$ vs. temperature for all the membranes are shown in Fig. 3. As is evident from the plot, Nafion® 117 exhibited the highest $I_d$ over the whole temperature range, SPES-40 showed lower values than SPES-PS. Based on Eq. (1), the magnitude of $I_d$ is affected by the product of $D$ and $C$. The magnitude of

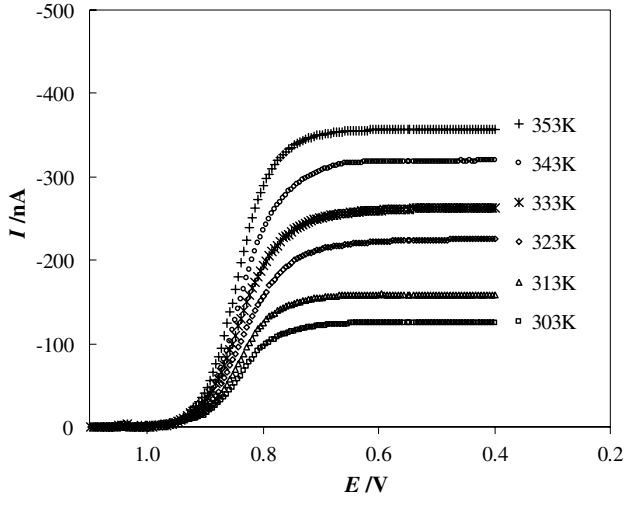


Fig. 2. Representative plots showing slow-sweep voltammograms for $O_2$ reduction at a Pt microelectrode|SPES-40 membrane interface under conditions of 100% relative humidity (RH), in the temperature range 303–353 K, 3 atm $O_2$ pressure (total pressure); scan rate = 2 mV $s^{-1}$.

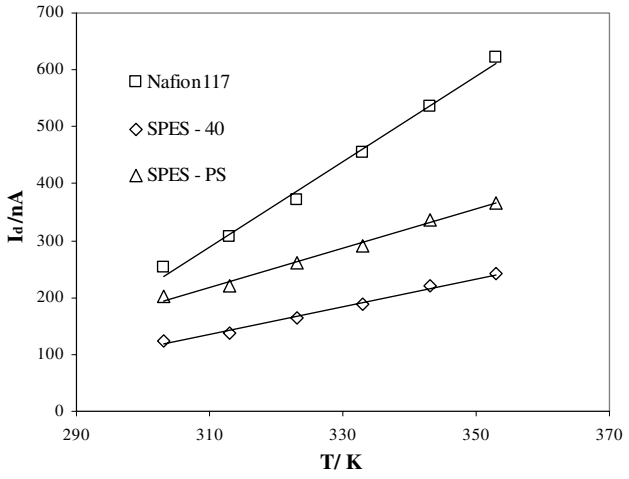


Fig. 3. Plots of limiting current, $I_d$ (nA), vs. temperature (K) for a Pt microelectrode|proton exchange membrane (PEM) interface under conditions of 100% RH, as a function of temperature (303–353 K), 3 atm $O_2$ pressure (total pressure).

the $I_d$ values therefore provides an overview of the relative differences in $O_2$ permeability (*DC*).

Earlier kinetic investigations on Pt/liquid acid electrolytes [46,47] as well as at the Pt|Nafion® 117 interface [33,36] have shown a break in the mass-transport corrected Tafel plots. The two sets of Tafel kinetic parameters at low and high current density domains correspond to the oxygen reduction reaction at oxide-covered and oxide-free surfaces of Pt [33]. Tafel plots for the perfluorinated polymer membrane Nafion® 117 and the two polymer membranes with aromatic chain backbones were generated using the mass-transport corrected Tafel equation (Eq. (2)). Fig. 4 shows the representative Tafel plots for (a) SPES-40 and (b) SPES-PS. The two well-defined linear regions in these plots were similar to previous reports [34,36]. Tafel parameters corresponding to each temperature are listed in Table 1. The exchange current densities for Nafion® 117 obtained in this investigation are comparable to previously published results by Parthasarathy et al. [34]. Comparison of the exchange current densities for all the membranes in the low current density (lcd) and high current density (hcd) regions, exhibited approximately the same order of magnitude, although Nafion® 117 showed slightly higher values than SPES-40 and SPES-PS membranes. The Tafel slopes for all the membranes studied show deviations from the "typical" number of −60 [46] (lcd) and −120 mV decade$^{-1}$ [47] (hcd). Further, the transfer coefficient $\alpha$ also exhibited some deviations from the characteristic value of 1 (lcd) and 0.5 (hcd). For example, the Tafel slopes for SPES-PS at lcd and hcd ranged from −71.5 to −77 mV decade$^{-1}$ and −106.8 to −116.6 mV decade$^{-1}$, respectively; its $\alpha$ values at lcd was in the range 0.84–0.91. Such deviations of the Tafel parameters from typical values are inherent in these

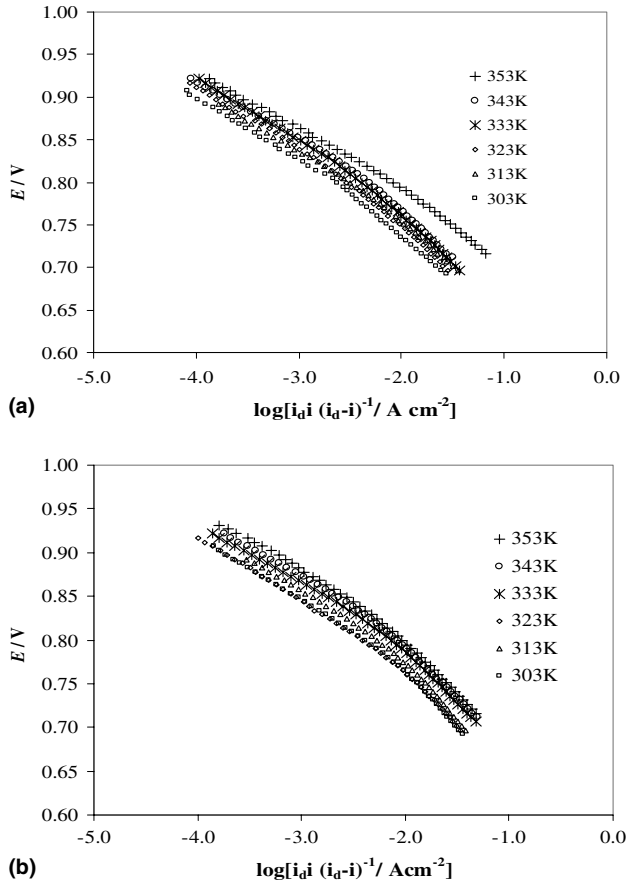


Fig. 4. Representative plots of mass-transport corrected Tafel plots for (a) SPES-40 and (b) SPES-PS membranes under conditions of 100% RH, as a function of temperature in the range of 303–353 K, 3 atm $O_2$ pressure (total pressure).

measurements as is evident from similar results on Nafion® 117. The exact cause is complex and difficult to control; prior reports such as those by Beattie et al. [36] have ascribed these variations to impurities in the membrane.

Table 1 shows that for all the membranes studied, the Tafel slopes at hcd (oxide free region), increase with temperature. Our data for Nafion® 117 are in agreement with those previously reported by Beattie et al. [36]. This increase with temperature was however less for the membranes with aromatic chain backbones. No such correlations could be made for the corresponding variation in the lcd region.

Correlation of the symmetry factor $\alpha$ with temperature has been interpreted in terms of Bockris–Gochev theory [48]. This theory, based on investigation at a Pt|trifluoromethanesulfonic acid (TFMSA) interface, at potentials greater than the potential of zero charge, suggests that the excess positive charge on the electrode is balanced by the negatively charged sulfonic acid groups in the electrolyte. Since these sulfonate anions are enclosed within the hydrophilic domains of the

Table 1
Electrode kinetic parameters for various PEM systems measured at the interface with a Pt microwire electrode (100 μm), studied as a function of temperature in the range 303–353 K, under conditions of 100% RH, 3 atm $O_2$ pressure (total pressure)

| Membrane | $T$ (K) | $E_r$ (V) | Tafel slope (lcd) (mV dec$^{-1}$) | $i_0$ (lcd) (nA cm$^{-2}$) | $\alpha$ (lcd) | $E_a$ (lcd) (kJ mol$^{-1}$) | Tafel slope (hcd) (mV dec$^{-1}$) | $i_0$ (hcd) (μA cm$^{-2}$) | $\alpha$ (hcd) | $E_a$ (hcd) (kJ mol$^{-1}$) |
|---|---|---|---|---|---|---|---|---|---|---|
| Nafion 117 | 303 | 1.303 | −69.9 | 1.95 | 0.86 | 26.76 | −108.5 | 0.553 | 0.55 | 36.03 |
| | 313 | 1.297 | −66.9 | 1.91 | 0.93 | | −114.6 | 1.24 | 0.54 | |
| | 323 | 1.292 | −70.4 | 6.65 | 0.91 | | −108.6 | 1.01 | 0.59 | |
| | 333 | 1.286 | −69.2 | 7.02 | 0.95 | | −109.9 | 1.44 | 0.60 | |
| | 343 | 1.281 | −70.5 | 10.1 | 0.97 | | −124.2 | 3.68 | 0.55 | |
| | 353 | 1.275 | −67.1 | 5.54 | 1.04 | | −123.3 | 4.65 | 0.57 | |
| SPES-40 | 303 | 1.303 | −72.6 | 0.273 | 0.83 | 28.5 | −100.7 | 0.0235 | 0.60 | 43.95 |
| | 313 | 1.297 | −71.2 | 0.333 | 0.87 | | −97.6 | 0.026 | 0.64 | |
| | 323 | 1.292 | −72.4 | 0.567 | 0.89 | | −104.4 | 0.0599 | 0.61 | |
| | 333 | 1.286 | −74.3 | 1.30 | 0.89 | | −105.6 | 0.0906 | 0.63 | |
| | 343 | 1.281 | −70.0 | 0.704 | 0.97 | | −108.3 | 0.178 | 0.63 | |
| | 353 | 1.275 | −67.9 | 0.840 | 1.03 | | −101.7 | 0.218 | 0.69 | |
| SPES-PS | 303 | 1.303 | −71.5 | 0.396 | 0.84 | 28.24 | −106.8 | 0.0826 | 0.56 | 40.55 |
| | 313 | 1.297 | −71.9 | 0.693 | 0.86 | | −109.1 | 0.145 | 0.57 | |
| | 323 | 1.292 | −73.8 | 0.867 | 0.87 | | −110.3 | 0.148 | 0.58 | |
| | 333 | 1.286 | −70.0 | 0.960 | 0.94 | | −112.4 | 0.344 | 0.59 | |
| | 343 | 1.281 | −70.9 | 1.72 | 0.96 | | −114.4 | 0.528 | 0.59 | |
| | 353 | 1.275 | −77.0 | 7.39 | 0.91 | | −116.6 | 0.789 | 0.60 | |

*Note*. All current densities were calculated relative to the real area of the working electrode. $E_r$ at different temperatures was calculated according to [36].

micelles formed by perfluorinated sulfonic acids such as TFMSA, some of the water molecules in the aqueous domains interact with the $SO_3^-$ via hydrogen bonding. Attempts to correlate the symmetry factor $\alpha$ with temperature however did not present any meaningful trends for Nafion® 117 and the membranes with aromatic chain backbones, which was true in both the current density regions (lcd and hcd). This is in agreement with prior publications where no such correlation with Nafion® 117 was also reported [36]. The anomalous dependence of the symmetry factor ($\alpha$) with temperature has been ascribed to changes in the hydrogen bonding with temperature.

The activation energies of oxygen reduction reaction, $E_a$ (kJ mol$^{-1}$), are also listed in Table 1. In both the lcd and hcd regions, Nafion® 117 exhibits slightly lower activation energies as compared to the membranes with aromatic chain backbones. SPES-40 and SPES-PS have very close $E_a$ values in both current density regions possibly due to their similar polymer structures. As reported previously by Sepa et al. [49], based on both experimental results and theoretical calculations, the difference between the activation energies in the lcd (oxide covered) and hcd (oxide free) regions should be 16 kJ mol$^{-1}$. This is based on the assumption that the first electron transfer step in both the regions is the rate determining step in accordance to the equation: $O_2 + H^+ + e^- \rightarrow O_2H_{ads}$. Our results show a difference in the range of 9.27 kJ mol$^{-1}$ for Nafion® 117 to 15.45 kJ mol$^{-1}$ for SPES-40, which are within the limits of error inherent in these measurements. Hence the kinetics observed at the Pt microelectrode interface for all the membranes agree well with well-established mechanistic interpretations for the orr, which considers the electron transfer step at both oxide covered and oxide free Pt surfaces to be rate determining. However, the observed deviations do not completely rule out the possibility of the chemical step being rate determining. A more careful evaluation of these kinetics is necessary for making such a definitive distinction.

### 3.2.2. Pressure dependence of the electrochemical reduction of $O_2$ at a Pt/PEM interface

After the temperature dependence study, the electrochemical cell system was cooled down to 303 K and equilibrated at ambient pressure. This equilibration at 100% RH, 303 K and 1 atm $O_2$ pressure was conducted for 24 h. This procedure helped to diminish the potential of a hysteresis effect on the electrode kinetic measurements. After full equilibration, the temperature of the system was increased to 323 K, and a pressure dependence study was conducted with the oxygen pressure varied between 1 and 4 atm (total pressure). Correction for oxygen partial pressure values was made taking into consideration the saturation vapor pressure of water (0.122 atm at 323 K and 1 atm [50]).

Fig. 5 shows representative slow sweep voltammograms at a Pt microelectrode|SPES-PS interface as a function of pressure. The limiting current $I_d$ associated with the reduction reaction displays an increasing trend

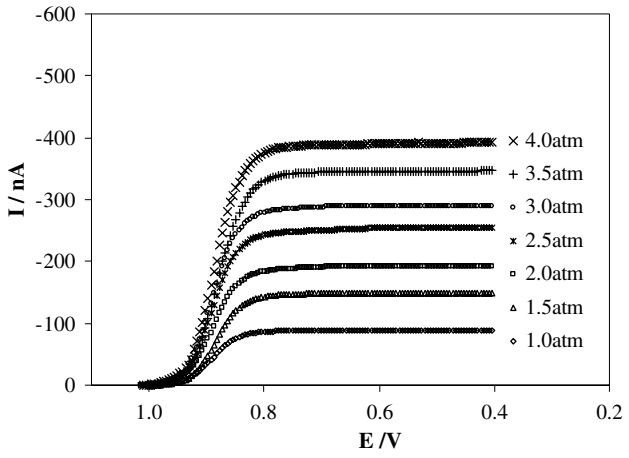


Fig. 5. Representative plot showing a slow-sweep voltammogram for $O_2$ reduction at the Pt microelectrode|SPES-PS membrane interface under conditions of 100% RH, in the pressure range 1–4 atm (total pressure), at 323 K temperature, scan rate = 2 mV $s^{-1}$.

with pressure. All the membranes studied gave similar responses. The $I_d$ values at 323 K and 3 atm $O_2$ pressure were close to those observed under the same conditions during our temperature dependence study, pointing to excellent reproducibility of the experimental set up. Plots of $I_d$ vs. partial pressure of oxygen ($PO_2$) for the three membranes are shown in Fig. 6. These plots demonstrate clear linear relationships, which are a consequence of Henry's law ($PO_2 = K_H C$, where $K_H$ is Henry's constant for the membrane) [51].

Mass-transfer corrected Tafel plots for the ORR were constructed from the pseudo-steady-state slow-scan voltammograms in accordance with the methods described previously [36]. Fig. 7 shows a representative Tafel plot as a function of $O_2$ pressure (total pressure) for the SPES-PS membrane. The two-slope Tafel plot is analogous to those observed in previous investigations [35,36]. The calculated kinetic parameters are given in Table 2. As expected, the exchange current densities increase with $O_2$ pressure for all the membranes in both lcd and hcd regions. At lcd, Nafion® 117 and the two SPES membranes exhibit exchange current densities roughly of the same order of magnitude, while in hcd, SPES-40 and SPES-PS show slightly better kinetics as compared to Nafion® 117.

The reaction order ($\rho$), for the ORR was determined from plots of $\log i_0$ vs. $\log PO_2$ in both the low and high current density regions, similarly to the procedure described earlier [52]. Good linear relationships were evident (Figs. 8(a) and (b)). As evident from the values given in Table 2, all the membranes exhibited values of $\rho$ close to 1 in both lcd and hcd regions, which confirms that $H_3O^+ + O_2 + e^- \rightarrow O_2H_{(ads)} + H_2O$ is the most likely rate determining step for the $O_2$ reduction reaction at the Pt|PEM interface. A reaction order of one is in agreement with prior reports on Nafion® 117 [35,36].

From an overall perspective, the results of the orr kinetics as a function of temperature and pressure show relatively small variations in electrode kinetics for all the three membranes.

### 3.3. Determination of mass-transport parameters by the chronoamperometric method

#### 3.3.1. Temperature dependence of the $O_2$ transport parameters at a Pt/PEM interface at 3 atm pressure

Microelectrode based chronoamperometric methods have been used extensively to determine the $O_2$ transport parameters (diffusion coefficient and solubility) for solid polymer electrolyte membranes; details of the measurements and data analysis are described elsewhere

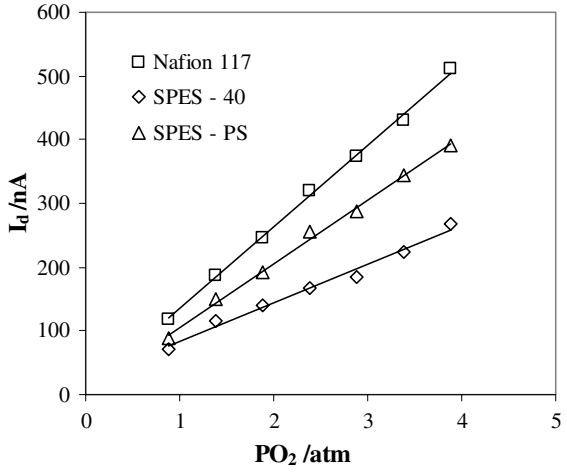


Fig. 6. Plots of limiting current, $I_d$ (nA) vs. partial pressure of oxygen measured at a Pt microelectrode|PEM interface under conditions of 100% RH, in the pressure range 1–4 atm (total pressure), 323 K temperature.

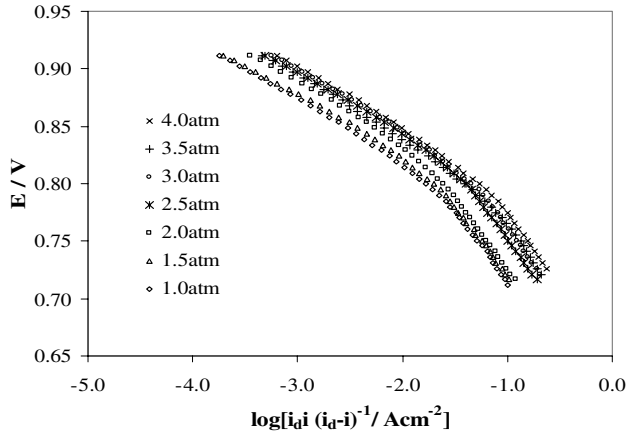


Fig. 7. Representative mass-transport corrected Tafel plots for the SPES-PS membrane under conditions of 100% RH, as a function of pressure in the range 1–4 atm (total pressure), at 323 K.

Table 2
Electrode kinetic parameters for various PEM systems at the interface with a Pt microwire (100 μm) working electrode, studied as a function of pressure in the range 1–4 atm (total pressure), under conditions of 100% RH, 323 K

| Membrane | $PO_2$ (atm) | $E_r$ (V) | Slope (lcd) (mV dec$^{-1}$) | $i_0$ (lcd) (nA cm$^{-2}$) | α (lcd) | ρ | Slope (hcd) (mV dec$^{-1}$) | $i_0$ (hcd) (μA cm$^{-2}$) | α (hcd) | ρ |
|---|---|---|---|---|---|---|---|---|---|---|
| Nafion 117 | 0.88 | 1.283 | −64.6 | 0.048 | 0.99 | 1 | −92.9 | 0.00379 | 0.69 | 1.03 |
| | 1.38 | 1.287 | −67.6 | 0.14 | 0.95 | | −95.0 | 0.00762 | 0.67 | |
| | 1.88 | 1.289 | −66.0 | 0.11 | 0.97 | | −96.1 | 0.00981 | 0.67 | |
| | 2.38 | 1.290 | −66.5 | 0.133 | 0.96 | | −97.7 | 0.0126 | 0.66 | |
| | 2.88 | 1.292 | −69.6 | 0.168 | 0.92 | | −99.4 | 0.0117 | 0.64 | |
| | 3.38 | 1.293 | −69.1 | 0.18 | 0.93 | | −96.8 | 0.011 | 0.66 | |
| | 3.88 | 1.294 | −70.3 | 0.318 | 0.91 | | −102.6 | 0.0279 | 0.62 | |
| SPES-40 | 0.88 | 1.283 | −69.3 | 0.463 | 0.92 | 0.96 | −141.6 | 0.704 | 0.45 | 0.98 |
| | 1.38 | 1.287 | −70.7 | 0.86 | 0.91 | | −142.2 | 0.718 | 0.45 | |
| | 1.88 | 1.289 | −71.9 | 1.24 | 0.89 | | −137.8 | 0.752 | 0.46 | |
| | 2.38 | 1.290 | −69.5 | 0.819 | 0.92 | | −142.1 | 1.40 | 0.44 | |
| | 2.88 | 1.292 | −69.0 | 0.949 | 0.93 | | −143.5 | 1.41 | 0.45 | |
| | 3.38 | 1.293 | −72.2 | 1.99 | 0.89 | | −146.5 | 1.72 | 0.44 | |
| | 3.88 | 1.294 | −73.6 | 2.70 | 0.87 | | −159.5 | 3.57 | 0.40 | |
| SPES-PS | 0.88 | 1.283 | −55.1 | 0.0355 | 1.16 | 1.2 | −115 | 1.14 | 0.56 | 1.17 |
| | 1.38 | 1.287 | −55.9 | 0.0478 | 1.15 | | −115.4 | 1.21 | 0.56 | |
| | 1.88 | 1.289 | −54.2 | 0.0561 | 1.18 | | −119.9 | 2.05 | 0.53 | |
| | 2.38 | 1.290 | −56.5 | 0.0754 | 1.13 | | −121.6 | 3.70 | 0.53 | |
| | 2.88 | 1.292 | −55.6 | 0.0899 | 1.15 | | −121.7 | 4.35 | 0.52 | |
| | 3.38 | 1.293 | −58.5 | 0.164 | 1.10 | | −122.1 | 4.42 | 0.52 | |
| | 3.88 | 1.294 | −58.7 | 0.236 | 1.09 | | −121.9 | 5.19 | 0.53 | |

[33,34,36]. Investigations on the effect of temperature on diffusion coefficients ($D$) and solubility of $O_2$ ($C$) in the polymer membranes, were conducted in the temperature range 303–353 K, at 3 atm $O_2$ pressure (total pressure) and 100% RH. Plots of $I$ vs. $t^{-1/2}$ for oxygen reduction at the Pt|PEM interface exhibit linear behavior (correlation coefficient $\geqslant 0.999$) between a time window of 1–5 s as represented in Fig. 9 under the conditions of 323 K and 3 atm $O_2$ pressure (total pressure).

The mass-transport values are tabulated in Table 3 and their variation with temperature is illustrated in Figs. 10(a)–(c). For all the membranes, the diffusion coefficient $D$ is observed to increase with temperature, while the opposite trend is true for the solubility $C$. Similar observations have been made previously for Nafion® 117 and BAM® 407 membranes [34,36]. Further, the increase in $D$ with temperature is greater than the decrease in $C$. As a result, the overall permeability ($DC$) increases linearly with temperature. The principal features evident from the plots shown in Figs. 10(a)–(c) are: (i) over the temperature range (303–353 K), Nafion® 117 exhibits a much greater change of diffusion coefficient as compared to the SPES membranes; (ii) a smaller difference in the variation of diffusion coefficient with temperature was observed in the two SPES membranes, in the ascending order SPES-PS > SPES-40; (iii) the variation in solubility as a function of temperature in descending order was Nafion® 117 > SPES-PS > SPES-40; (iv) the overall permeability of Nafion® 117 is significantly higher as compared to the SPES membranes and exhibits a higher slope in its variation. For the two SPES membranes, SPES-PS exhibited higher permeability and slope as compared to SPES-40. Comparison of both diffusion coefficients and solubility for Nafion® as a function of temperature at 3 atm with prior published data from Beattie et al. [36] and Parthasarathy et al. [34] showed reasonable agreement.

Plots of $\log D$ and $\log C$ vs. $T^{-1}$ ($10^3$) shown in Fig. 11 exhibit linear dependences over the temperature range investigated (303–353 K, 3 atm), which are in agreement with our previous work at ambient pressure conditions [40]. Prior publications by Parthasarathy et al. [34] and Beattie et al. [36], have reported a break in their Arrhenius plots showing evidence of two separate linear regions between 303–323 and 323–343 K. This has been explained on the basis of a similar break in the water uptake values as a function of temperature. Our data on the water uptake (Table 4), however, did not show such a break for any of the membrane studied. Note that our water uptake measurements for Nafion® 117 agree very well with those reported by Hinatsu et al. [53]. This largely explains the continuous linear trend of both $D$ and $C$ as a function of temperature for the membranes in this study. This linear behavior is also confirmed by examining the water uptake data expressed in terms of variation of $\lambda$ with temperature. As shown in Fig. 12 single linear behavior is observed. Such a single linear variation with temperature allowed for unique activation energy values for $O_2$ diffusion ($E_d$) and the enthalpy of solubilization of $O_2$ in the membranes ($\Delta H_s$) to be

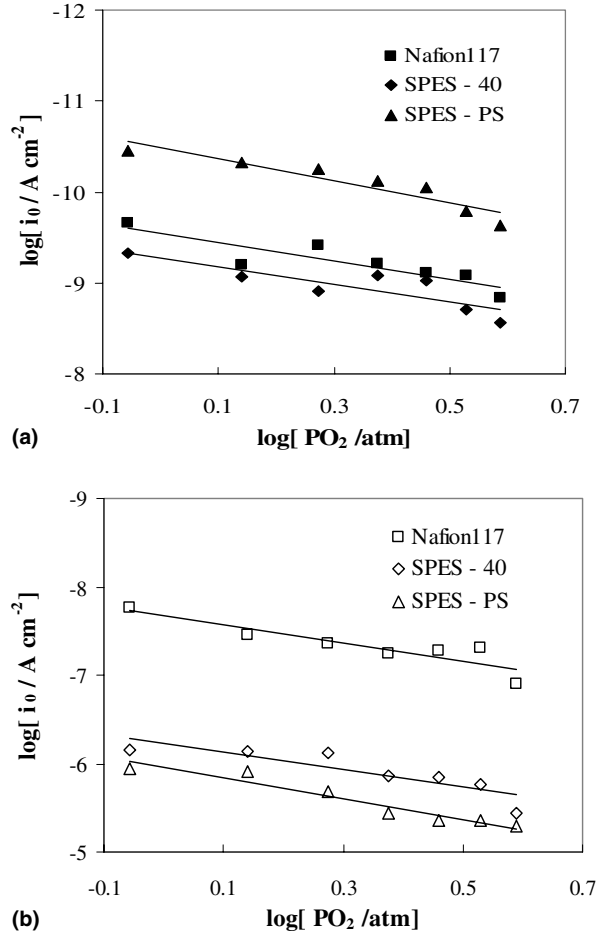


Fig. 8. A log–log plot of $I_0$ vs. $PO_2$ (partial pressure of oxygen) for Pt microelectrode|PEM interface studied in (a) the low current density (lcd) region; and (b) the high current density (hcd) region.

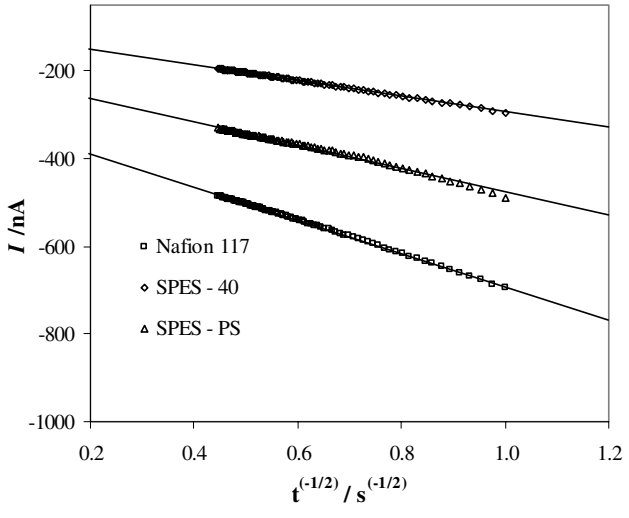


Fig. 9. Representative $I$ (nA) vs. $t^{-1/2}$ plots for oxygen reduction at the Pt microelectrode|PEM interface under 100% RH, 3 atm (total pressure) and 323 K.

determined (Table 5). This is in contrast to two sets of values in each linear region reported earlier [34,36].

The temperature variation of mass-transport parameters of SPES-40 and SPES-PS and its relationship with Nafion® 117 can be explained on the basis of the microstructure of the swollen membranes. It is well established that perfluorinated sulfonic acid membranes such as Nafion® are phase-separated materials. They are comprised of amorphous hydrophobic Teflon backbone regions and hydrophilic ionic domains containing randomly attached pendant chains terminated with sulfonic acid groups [37]. These are based on a wealth of earlier work such as that by Gierke et al. [54–56] which has established the formation of ionic clustering in these materials. The microstructure model, which has emerged, suggests the formation of inverted micelles with $SO_3^-$ groups forming hydrated clusters embedded in a fluorocarbon phase with diameters of 30–50 Å as confirmed by small angle X-ray scattering (SAXS) [57,58]. Recent AFM imaging studies [32] using a tapping mode have shown the existence of roughly two phases in the SPES membranes. These are the ionic cluster phase, comprising of hydrophilic sulfonic acid groups, which contains most of the associated water and the non-ionic matrix phase, which may be assigned to the relatively hydrophobic aromatic backbone. Earlier reports [33,34,37] have shown that water acts as a plasticizer in Nafion® and hence increase of the water content enables increase in the diffusion coefficient of oxygen. The opposite is true for the solubility [33,34,37], where the solubility of oxygen was determined by the fraction of the hydrophobic component in the membrane. Hence, shrinking of the hydrophobic phase leads to a decrease in $O_2$ concentration, since $O_2$ tends to be more soluble in hydrophobic domains than in hydrophilic parts [59].

As pointed out earlier [60], the water content in the membrane is determined by a combination of three processes: (i) water sorption by the membrane, which is controlled by its ion exchange capacity (number of ionic groups per unit weight); (ii) its electroosmotic drag coefficient, which is a function of its proton conductivity; and (iii) water diffusion caused by gradients in the water activity. This role of water content as determined by its equivalent weight (EW) has been demonstrated earlier using a comparison of sulfonated α, β, β-trifluorostyrene (BAM®, Ballard, Canada) membranes with Nafion® 117 as well as an investigation on perfluorinated sulfonic acid membranes as a function of equivalent weight (Nafion® series as well as Aciplex membranes). A comparison of BAM® 407 (EW = 407) with Nafion® 117 (EW = 1100) showed the expected result of higher diffusion coefficient and lower solubility (approximately four times) for BAM® 407 relative to Nafion® 117 [36]. This was rationalized purely on the basis of water content in these membranes (87 wt% for BAM® 407

Table 3
Comparison of mass-transport properties for various PEM systems studied as a function of temperature in the range 303–353 K, under conditions of 100% RH, 3 atm $O_2$ pressure (total pressure)

| $T$ (K) | Nafion 117 | | | SPES-40 | | | SPES-PS | | |
|---|---|---|---|---|---|---|---|---|---|
| | $10^6 D$ ($cm^2\ s^{-1}$) | $10^6 C$ ($mol\ cm^{-3}$) | $10^{12} DC$ ($mol\ cm^{-1}\ s^{-1}$) | $10^6 D$ ($cm^2\ s^{-1}$) | $10^6 C$ ($mol\ cm^{-3}$) | $10^{12} DC$ ($mol\ cm^{-1}\ s^{-1}$) | $10^6 D$ ($cm^2\ s^{-1}$) | $10^6 C$ ($mol\ cm^{-3}$) | $10^{12} DC$ ($mol\ cm^{-1}\ s^{-1}$) |
| 303 | 3.06 | 11.24 | 34.44 | 1.24 | 9.84 | 12.22 | 1.95 | 11.58 | 22.57 |
| 313 | 3.88 | 10.51 | 40.82 | 2.55 | 6.41 | 16.38 | 2.90 | 9.25 | 26.82 |
| 323 | 5.51 | 9.42 | 51.88 | 3.34 | 5.69 | 19.04 | 4.88 | 7.06 | 34.51 |
| 333 | 7.81 | 8.52 | 66.51 | 4.56 | 5.10 | 23.25 | 5.96 | 6.54 | 39 |
| 343 | 10.67 | 7.47 | 79.75 | 5.87 | 4.40 | 25.82 | 7.27 | 6.20 | 45.05 |
| 353 | 12.51 | 7.08 | 88.55 | 7.72 | 3.90 | 30.07 | 10.32 | 5.09 | 52.54 |

The reported values are the average of three separate experiments for each PEM system.

compared to 19 wt% for Nafion® 117 at 50 °C) [36]. This is also evident when comparing this effect for a particular family of membranes as a function of EW or water content. Prior results with BAM® (Ballard, Canada), DIAS® (DIAS Analytic, USA), Nafion® (Dupont, USA) and Aciplex® (Asahi chemicals, Japan) [37,39] show a remarkable correlation with water content within each family of membranes. An estimation of this effect has been made using the extent of variation in the hydrophilic phase between membranes with different equivalent weights [37]. In this case a gravimetric density of 2.2 g $cm^{-2}$ was assumed for the hydrophobic phase and 1.0 g $cm^{-2}$ for the hydrophilic phase. For the hydrophobic phase the model system chosen was polytetrafluoroethylene (PTFE®). This is supported by earlier work by Ogumi et al. [61], who found identical $O_2$ solubility and diffusion coefficient for dry Nafion® 125 and PTFE membranes. For the hydrophilic phase, the values reported in 1 M $H_2SO_4$ were used in the calculations. At 323 K, the $D$ and $C$ for $O_2$ in PTFE® is reported to be $0.35 \times 10^{-6}$ $cm^2\ s^{-1}$ and $37 \times 10^{-6}$ mol $cm^{-3}$. The corresponding values for $O_2$ in 1 M $H_2SO_4$ are $31 \times 10^{-6}$ $cm^2\ s^{-1}$ and $5 \times 10^{-6}$ mol $cm^{-3}$.

Correlation of water contents and the variation of mass-transport parameters with temperature (Figs. 10(a)–(c)) show interesting trends. As mentioned above, Fig. 10(a) shows that Nafion® 117 exhibits the highest $D$ over the entire temperature range; the SPES membranes have lower values in the descending order SPES-PS > SPES-40. In addition, the slope of the variation of $D$ with temperature is highest for Nafion® 117 with the SPES membranes showing significantly lower slopes in the same descending order. These results cannot be accounted for on the basis of water content (or IEC) alone. As illustrated in Table 5, Nafion® 117 has the lowest IEC at any temperature (meq $g^{-1}$) of all the membranes used in this investigation (0.91 vs. 2 for SPES-PS, 1.72 for SPES-40 at 25 °C). Hence the water uptake of SPES-PS, SPES-40 is significantly higher than that of Nafion® 117 as shown in Tables 4 and 5. However, despite the higher water content, the $O_2$ diffusion coefficients of all the hydrocarbon membranes are lower, e.g., the SPES-40 membrane at 323 K has a diffusion coefficient of $3.34 \times 10^{-6}$ $cm^2\ s^{-1}$ as compared to Nafion® 117 ($D = 5.51 \times 10^{-6}$ $cm^2\ s^{-1}$). Comparison of the percentage volume of the aqueous phase at 50 °C shows that the SPES membranes exhibit approximately double the value as compared to Nafion® 117 (Table 5).

Although the wealth of prior results seems to indicate that water plays a central role in determining the $O_2$ permeation in proton exchange membranes, its exact mechanism remains unclear and deserves further investigation. It is evident in this comparison that SPES-40 and SPES-PS membranes have widely different chemical structure as compared to Nafion® 117. The hydrophobicity of the aromatic backbone of these SPES membranes is not as strong as for Nafion®, with its perfluorinated backbone, and the sulfonic acid functional groups in these SPES membranes are less acidic than in Nafion®. Therefore, one may expect a less pronounced hydrophilic/hydrophobic separation in these membranes as compared to Nafion® 117. Such behavior has been observed with the related sulfonated poly(ether ether ketone) system using SAXS [62]. As a result, one must use caution when comparing the mass-transport characteristics of membranes with respect to differences in their water uptake alone. The difference in chemistry is also expected to play an important role.

AFM image analysis using tapping mode [32], shows some striking results concerning the morphologies of the ionic phases. For the SPES-40 membrane, the hydrophilic ionic domains are isolated and dispersed among the non-ionic matrix domains with an average of 25 nm diameter [32]. In contrast, the image of Nafion® 117, is reported to have significantly smaller hydrophilic ionic domains (about 10 nm) which tend to form continuous channels in the structure [32]. Assuming that $O_2$ diffusion is predominantly related to water content, the well-connected channels between ionic domains of Nafion® 117 may form a three-dimensional water network, which seems a more favorable transport pathway for $O_2$. As for SPES-40, despite the larger size of the hydrophilic clusters, the water filled channels may be narrower or more branched with a greater number of dead-ends; $O_2$

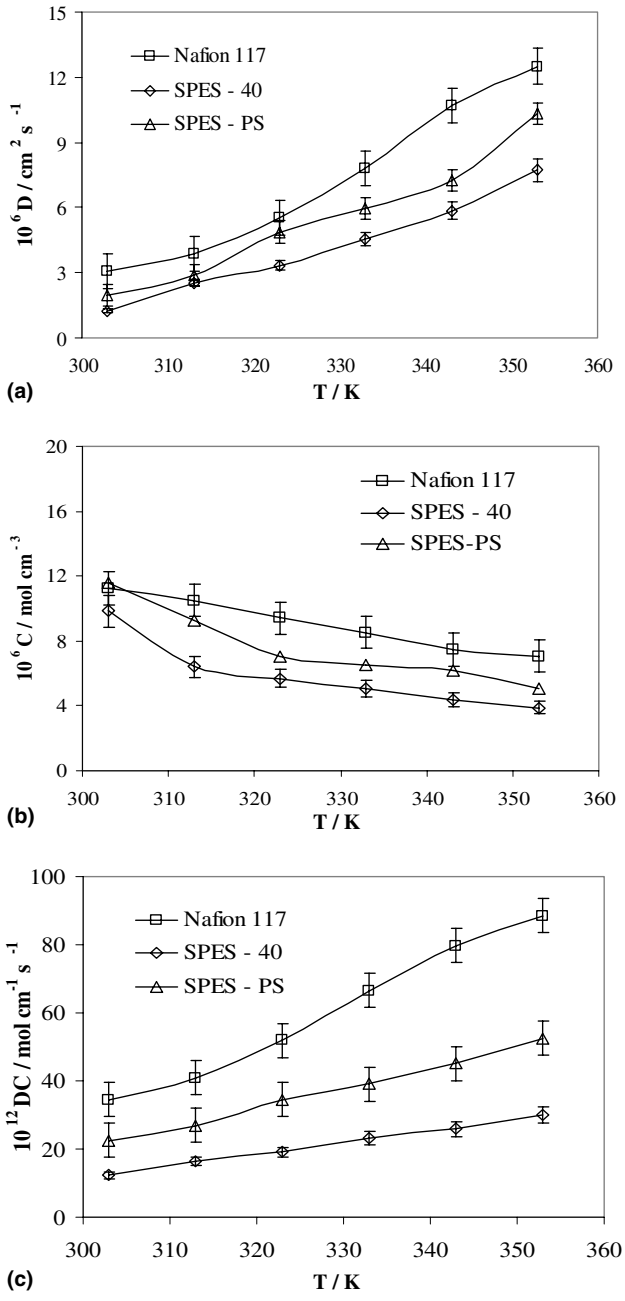


Fig. 10. Temperature (K) vs. (a) diffusion coefficient ($D$), (b) solubility ($C$), and (c) permeability ($DC$) of oxygen at the Pt microelectrode|PEM interface studied under conditions of 100% RH, pressure range 1–4 atm (total pressure), 323 K. The error bars represent the scatter in data for each PEM system based on a set of three separate experiments.

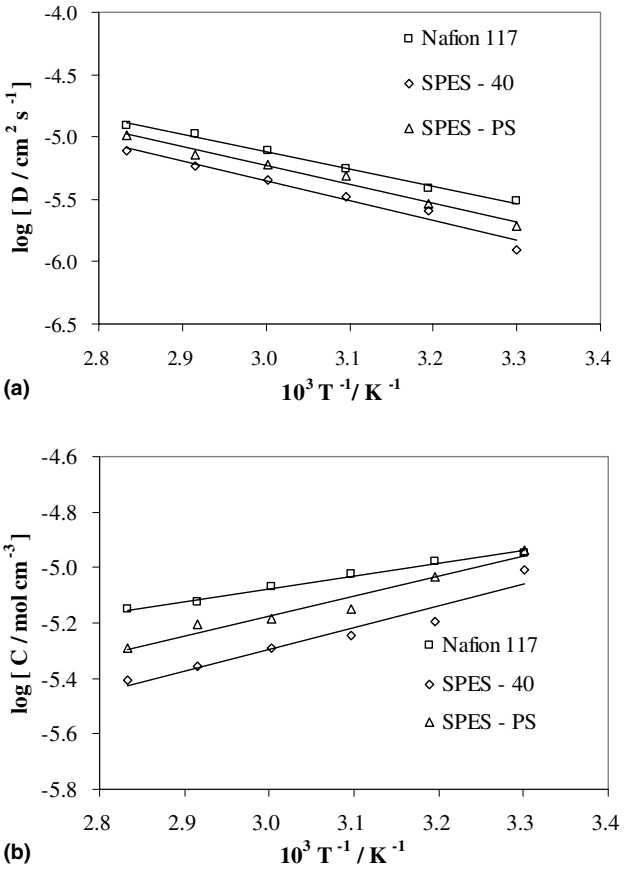


Fig. 11. Arrhenius plots of (a) $\log D$ and (b) $\log C$ vs. $1000/T$ for various Pt microelectrode|PEM interfaces studied under conditions of 100% RH, temperature range 303–353 K, 3 atm $O_2$ pressure (total pressure). The values of $D$ and $C$ are the averages of three separate experimental data sets for each membrane system.

therefore becomes blocked to a larger extent within SPES-40, thus leading to a relatively smaller increase in the diffusion coefficient despite the higher water content in the membrane.

SPES-40 and SPES-PS membranes possess similar polymer backbones and have very close $\lambda$ values as shown in Fig. 12 and Table 4. Therefore, despite a higher IEC and consequently greater water uptake as compared to SPES-40, the diffusion coefficient of SPES-PS is still lower than Nafion® 117. As for the comparison between SPES-PS and SPES-40, because of the inherent variations in the sulfonation level (IEC) as well as the positions of the sulfonic acid groups, the morphologies of the ionic cluster phases and the non-ionic matrix phases within SPES-PS may not be exactly similar to SPES-40. Apparently there are certain improvements in the connectivity between the ionic clusters in the SPES-PS membrane due to the higher water uptake: probably the hydrophilic ionic domains begin to form continuous channels, which contribute to faster oxygen diffusion in SPES-PS membranes. This proposed explanation requires further investigation since, to the best of our knowledge, there is no literature related to the microstructure of SPES-PS. However, SPES-PS (post-sulfonated) possesses only one sulfonic acid group on the activated ring next to the aromatic ether bond in every sulfonated unit, as opposed to two sulfonic acid groups in SPES-40 [32] (see structures in Section 2), so the acidity of the pendant groups in SPES-40 is expected to be modestly higher than those in SPES-PS due to the strong electron-withdrawing effect of the sulfone group.

Table 4
Water uptake values as a function of temperature in the range 298–373 K for various PEM membranes

| $T$ (°C) | Nafion 117 | | SPES-40 | | SPES-PS | |
|---|---|---|---|---|---|---|
| | Water uptake (wt%) | $\lambda$ | Water uptake (wt%) | $\lambda$ | Water uptake (wt%) | $\lambda$ |
| 25 | 20 | 12.5 | 65 | 21.1 | 71 | 19.6 |
| 40 | 25 | 15.4 | 73 | 23.4 | 75 | 21 |
| 50 | 27 | 16.2 | 78 | 25.2 | 79 | 22 |
| 60 | 28 | 17.1 | 80 | 25.9 | 80 | 22.1 |
| 70 | 31 | 18.7 | 83 | 27 | 84 | 23.3 |
| 80 | 35 | 21.1 | 85 | 27.3 | 88 | 24.8 |

The data are reported both as water uptake in wt% and in terms of $\lambda = (\mathrm{molH_2O/molSO_3^-})$.

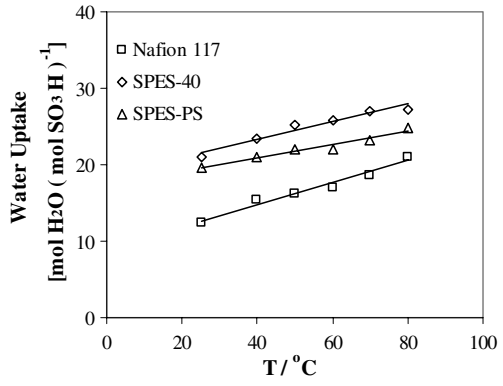


Fig. 12. Water uptake (expressed as number of moles of water/$SO_3^-$ group, $\lambda$) for various PEM membranes as a function of temperature.

This may be attributed to different degrees of hydrophobic/hydrophilic separations in the microstructures of these two membranes. Moreover, various factors such as copolymer composition [63], specific interactions between components [64] and membrane formation procedures as well as hydrothermal history [65] can influence the morphology of the sulfonated aromatic proton exchange membranes.

Comparison of diffusion coefficients at any point in the temperature range within the family of the SPES membranes shows good correlation with their corresponding IEC values. This is reflected in the data shown in Table 5. Comparison of the diffusion coefficient $D$ for Nafion® 117 and the two SPES membranes shows very good correlation with the corresponding activation energy of $O_2$ diffusion $E_d$, which can be arranged in ascending order as Nafion® 117 (26.5 kJ $mol^{-1}$) < SPES-PS (28.82 kJ $mol^{-1}$) < SPES-40 (30.56 kJ $mol^{-1}$).

In terms of solubility, comparison of data for Nafion® 117 and SPES membranes shows progressively lower values of oxygen solubility for SPES-40 and SPES-PS. The variation of solubility with temperature follows the same trend as the corresponding variation of the percentage aqueous phase. This has been shown earlier for a SPES-40 membrane under ambient pressure conditions [40] and for a BAM® (Ballard, Canada) membrane with EW = 407. In the latter case the comparisons were made under 3 atm pressure conditions. Even though reasonable correlation with equivalent weight of the membrane and its corresponding oxygen solubility exits in this case, the impact of the fundamental distinctions in their chemistry cannot be ruled out. As for the comparison between SPES-PS and SPES-40, SPES-PS has a slightly higher IEC and water content than SPES-40, but the oxygen solubility for SPES-PS is much higher than that of SPES-40. The cause of this phenomenon is not clear. A possible reason may be due to the different sulfonation sites and alternate patterns of repeat units in the backbone, since the solubility of oxygen in these membranes is mainly related to the hydrophobic domains.

The value for the enthalpy of dissolution, $\Delta H_s$, obtained from the corresponding Arrhenius plot of solubility ($C$) for Nafion® 117 is −8.73 kJ $mol^{-1}$, very close to a result published previously (−8.1 kJ $mol^{-1}$ [36]). The positive slopes of the van't Hoff plots ($\log C$ vs. $T^{-1}$), indicate negative values for both $\Delta H_s$ and $\Delta S_s$ (from the intercept); these have implications in terms of

Table 5
Comparison of $O_2$ transport parameters measured under conditions of 100% RH, 323 K, 3 atm $O_2$ pressure (total pressure) for various PEM systems

| Membrane | IEC (Meq $g^{-1}$) | Water uptake (wt%) | Volume of aqueous phase (%) | $10^6 D$ ($cm^2$ $s^{-1}$) | $10^6 C$ (mol $cm^{-3}$) | $10^{12} DC$ (mol $cm^{-1}$ $s^{-1}$) | $E_d$ (kJ $mol^{-1}$) | $\Delta H_s$ (kJ $mol^{-1}$) |
|---|---|---|---|---|---|---|---|---|
| Nafion 117 | 0.91 | 27 | 37.3 | 5.51 | 9.42 | 51.88 | 26.5 | −8.73 |
| SPES-40 | 1.72 | 78 | 63.2 | 3.34 | 5.69 | 19.04 | 30.56 | −15.06 |
| SPES-PS | 2 | 79 | 63.5 | 4.48 | 7.06 | 34.51 | 28.82 | −13.78 |

Also included are the corresponding data for ion exchange capacity, water uptake at 323 K and the volume of the aqueous phase. The values of the activation energy for oxygen diffusion and the enthalpy of dissolution are also given.

Table 6
Comparison of mass-transport properties for various PEM systems studied as a function of pressure in the range 1–4 atm ($O_2$ total pressure), under conditions of 100% RH, 323 K

| $PO_2$ (atm) | Nafion 117 | | | SPES-40 | | | SPES-PS | | |
|---|---|---|---|---|---|---|---|---|---|
| | $10^6 D$ ($cm^2\ s^{-1}$) | $10^6 C$ ($mol\ cm^{-3}$) | $10^{12} DC$ ($mol\ cm^{-1}\ s^{-1}$) | $10^6 D$ ($cm^2\ s^{-1}$) | $10^6 C$ ($mol\ cm^{-3}$) | $10^{12} DC$ ($mol\ cm^{-1}\ s^{-1}$) | $10^6 D$ ($cm^2\ s^{-1}$) | $10^6 C$ ($mol\ cm^{-3}$) | $10^{12} DC$ ($mol\ cm^{-1}\ s^{-1}$) |
| 0.29[a] | 1.01 | 3.58 | 3.64 | 0.70 | 1.82 | 1.27 | | | |
| 0.50[a] | 1.90 | 4.06 | 8.11 | 1.13 | 2.11 | 2.37 | | | |
| 0.71[a] | 2.58 | 4.49 | 11.61 | 1.44 | 2.97 | 4.27 | | | |
| 0.88 | 2.77 | 5.32 | 14.75 | 1.43 | 4.38 | 6.25 | 1.74 | 5.34 | 9.31 |
| 1.38 | 4.87 | 5.62 | 27.34 | 2.41 | 4.52 | 10.89 | 3.02 | 5.48 | 16.56 |
| 1.88 | 5.48 | 6.35 | 34.81 | 3.27 | 4.63 | 15.11 | 3.87 | 5.76 | 22.3 |
| 2.38 | 5.78 | 7.86 | 45.4 | 3.88 | 4.82 | 18.7 | 5.12 | 5.77 | 29.55 |
| 2.88 | 6.08 | 8.98 | 54.64 | 4.26 | 5.12 | 21.84 | 5.92 | 6.08 | 35.99 |
| 3.38 | 6.1 | 10.16 | 62.03 | 4.44 | 5.76 | 25.57 | 7.46 | 6.19 | 46.2 |
| 3.88 | 6.34 | 11.38 | 72.07 | 5 | 5.99 | 29.91 | 8.54 | 6.24 | 53.27 |

For Nafion® 117 and SPES-40, mass-transport result under 100% RH, 323 K and 1.5–3.5 atm pressure (air, total pressure) are included. The reported values are the average of three separate experiments for each PEM system.
[a] Work with air. Oxygen pressure = 0.209 (total pressure − water vapor pressure).

the interaction of the aqueous and non-aqueous phases in the membrane and the effect of different membrane chemistry. A negative value for $\Delta S_s$ for oxygen dissolution can be regarded as an ordering process. As pointed out earlier [34,36], a negative value of oxygen dissolution can be expected based on the negative entropy of dissolution at both the extreme ends of the phases of Nafion® (PTFE®, non-aqueous phase and $H_2SO_4$, aqueous phase). Therefore unique spatial arrangements of oxygen are expected between the aqueous and non-aqueous components of both Nafion® 117 and SPES. The higher values of $\Delta H_s$ and $\Delta S_s$ for SPES-PS and SPES-40 as compared to Nafion® 117, indicate a greater degree of spatial rearrangement during oxygen solubility in the SPES membranes. The exact mechanism of these interactions however awaits a molecular modeling study.

### 3.3.2. Pressure dependence of the $O_2$ transport parameters at a Pt/PEM interface

The pressure dependence of the gas transport parameters at a Pt|PEM interface was studied at 323 K as a function of $O_2$ pressure using chronoamperometry methods with the partial pressure of oxygen, $PO_2$ varied between 0.88 and 3.88 atm, which corresponds to a total pressure range of 1–4 atm. The methodology used was similar to that described in detail elsewhere [35,36,39]. Limiting currents, $I_d$, obtained from slow sweep voltammograms were measured as a function of $PO_2$ (after correction of saturated vapor pressure, 0.122 atm at 323 K at 1 atm pressure). To determine the mass-transport properties at $O_2$ partial pressures of less than 1 atm, independent experiments using humidified air were also conducted for SPES-40 and Nafion® 117 membranes. The results are tabulated in Table 6 and plotted in Figs. 13(a)–(c). As mentioned earlier, all membranes exhibited a linear response for the variation of limiting current and oxygen partial pressure (Fig. 6), which is in agreement with Henry's law.

Fig. 13(a) shows an increase of oxygen solubility $C$ with pressure for all the membranes in accordance to Henry's law. $C$ for the Nafion® 117 membrane, however, exhibited a much higher variation with pressure as compared to the SPES membranes. It is interesting to note that an extrapolation of $C$ vs. $PO_2$ (pure $O_2$) data to the origin (zero $PO_2$) for all membranes studied provides a positive intercept, thereby implicating non-zero solubility values. This is in contravention to a simple application of Henry's law. Our data for Nafion® 117 are in agreement with those reported earlier [35,36]. The corresponding behavior for SPES type membranes can be examined in the context of data reported for other alternative membranes such as those for BAM® (Ballard, Canada) and DAIS® membranes [36,38]. In this case comparison of the plots of solubility with $PO_2$ shows significantly smaller variation for membranes with similar EW and IEC as the SPES membranes in this study. It is interesting to note that these membranes possess either fluorinated (such as in the BAM® membrane) or non-fluorinated aliphatic polymer backbones (in DAIS® membranes) in contrast to the aromatic backbone of SPES membranes. In addition they all possessed pendant chains with sulfonic acid groups (Nafion®, BAM®, DAIS®) in contrast to direct sulfonation of the aromatic polymer backbone in the case of SPES membranes. The experiment with air on the SPES-40 membrane was designed to give some insight into this behavior. As shown in Fig. 13(a), the oxygen solubility in SPES-40 increased more rapidly in the $PO_2 < 1$ atm region than for $PO_2 > 1$ atm. There appears to be a break in the variation of $C$ with $PO_2$ centered at the corresponding change in total pressure of 1 atm. This could imply a change in the polymer microstructure brought about by pressure. Such a change in micro-

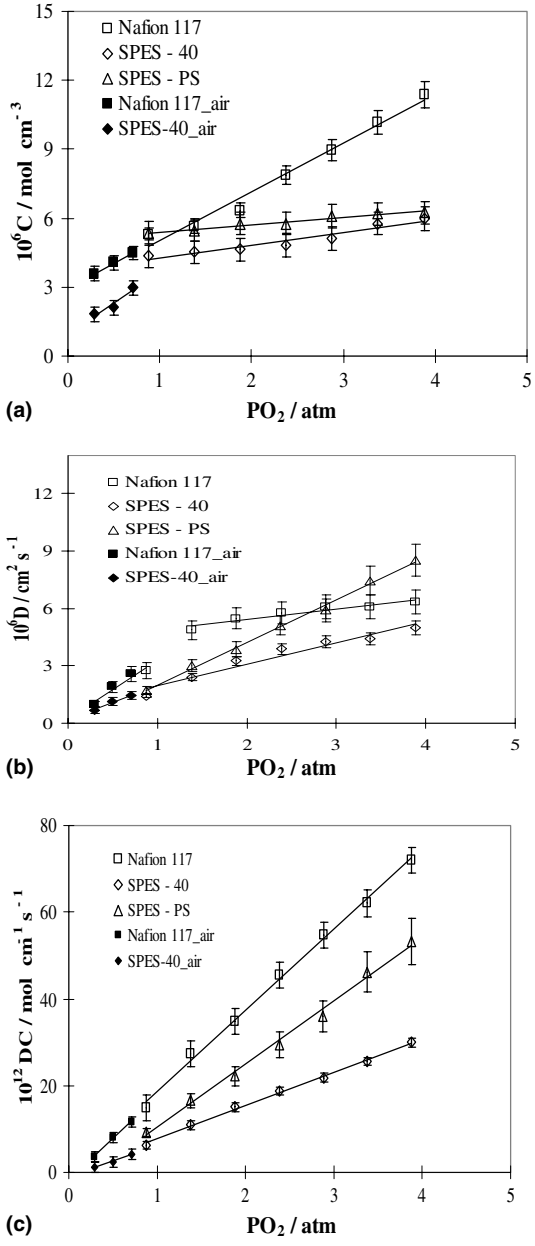


Fig. 13. Pressure vs. (a) solubility ($C$), (b) diffusion coefficient ($D$), and (c) permeability ($DC$) of oxygen at the Pt microelectrode|PEM interface studied under conditions of 100% RH, temperature range 303–353 K, 3 atm $O_2$ pressure (total pressure). The error bars represent the scatter in data for each PEM system based on a set of three separate experiments.

structure has been reported previously for Nafion® membranes [39], where a conversion from the N-form of the membrane to the more expanded E-form is reported. In our case, the break in the case of Nafion® 117 below $PO_2$ of approximately 1 atm is less than for SPES type membranes. A more pronounced break is reported by Basura et al. [39], which is accounted for on the basis of differences in thermal cycling of the Nafion® 117 membrane.

The plots of diffusion coefficient as a function of $PO_2$ are shown in Fig. 13(b). Two separate linear variations of $D$ with pressure were found for Nafion® 117 with a break at $PO_2$ of 1.5 atm, an initial rapid increase ($PO_2 < 1.5$ atm) followed by a leveling off beyond $PO_2$ of 1.5 atm. For the SPES-40 and SPES-PS membranes, $D$ increased approximately linearly with pressure. These reproducible results on SPES membranes are in contrast with previously reported data by Parthasarathy et al. [35], where the $O_2$ diffusion coefficient was reported to be independent of pressure for Nafion® 117 in the pressure range of 2–4 atm ($PO_2$). Our results on SPES membranes however are similar to those reported earlier by Beattie et al. [36] in the 2–4 atm pressure range and Basura et al. [39]. Basura et al. [39], have compared the mass-transport properties of $O_2$ for a series of BAM® and DAIS® membranes; here a consistent increase of $D$ with pressure (2–5 atm) was observed for all the membranes investigated, similar to our observation on SPES type membranes. Our data on the variation of diffusion coefficient as a function of pressure, showing a greater variation of diffusion coefficient with pressure in the range below 1.9 atm ($PO_2$) for Nafion® 117 and a leveling off beyond 1.9 atm agree well with prior data by Parthasarathy et al. [35]. However our data in the lower pressure range are more extensive and show this phenomenon more clearly.

As proposed in our earlier discussions on the data for temperature dependence of $D$ and $C$, arguments based on differences in the microstructure of the membranes (Nafion® vs. SPES) could account for differences in $O_2$ transport parameters as a function of pressure. Note that in our pressure dependence investigations, the temperature of the electrochemical cell system was fixed as 323 K; therefore the water content of the membranes should remain relatively constant in the entire pressure range. As mentioned previously [35,36], earlier work on perfluorinated sulfonic acid type membranes has ascribed the $O_2$ diffusion process to the nature of the hydrophilic ionic domains and hence on the water content of the membrane. This has been used in earlier reports to account for the weak dependence of pressure on the diffusion coefficients of Nafion® 117 [35,36]. Our observations on Nafion® 117 in the pressure range of 2–4 atm, is in agreement with these prior reports [35,36]. However, for the SPES membranes, and Nafion® 117 in the pressure range below 2 atm, variation of the microstructure with pressure may play a more important role in determining the $O_2$ diffusion processes, which appears to overshadow the influence of water content.

The exact reasons for these phenomena are not fully understood. As pointed out earlier in our discussions regarding variation of solubility with pressure, a change in microstructure of the membrane could occur as a result of pressurization. This has been shown to occur in the case of Nafion® 117, where, as mentioned

previously, a transformation from N to the more open E-form occurs as result of thermal cycling [39]. In the case of SPES membranes, the polymer backbone might be subject to certain rearrangements ending up with better conformation of the inter-chain channels or connections that facilitate the $O_2$ diffusion process as the pressure is increased. Further effort with the aid of molecular modeling and experimental investigations with tailored polymer synthesis is necessary for a better explanation of such variations with pressure. Some pointers to this can be gleaned from pressure-dependent sorption and transport of gases and vapor in industrial gas separation membranes. Based on $C^{13}$ NMR rotating-frame relaxation rate measurements, Raucher and Sefcik [66–68] elucidated that gas diffusion through the glassy polymers is controlled by the cooperative main chain motions of the polymer, and these motions are altered by the presence of solute [66,69]. This implies that sorbed gases can alter the structure and dynamics of the polymer matrix, thus altering the transport characteristics of the polymer system [66]. These studies had also proposed that gas–polymer interactions reduce the inter-chain potential of the polymer, thus decreasing the activation energy of polymer chain separation, and therefore the activation energy of diffusion [68]. The decrease in the activation energies results in higher frequencies of cooperative main chain motions and in higher diffusion coefficients [68].

Finally, as a consequence of the overall contributions from $D$ and $C$ as a function of pressure, the $O_2$ permeability (product $DC$) increases almost linearly with pressure (Fig. 13(c)). Nafion® 117 has approximately 1.5 times higher permeability than SPES-PS and 3 times higher than SPES-40 at 323 K over the pressure range 1–4 atm (total pressure). This relative magnitude mirrors the limiting current $I_d$ vs. pressure result described earlier. The lower solubility and permeability of oxygen in SPES-40, has very important implications for fabrication of practical membrane electrode assembly (MEA) using such materials. The choice of ionomer in the reaction layer of the electrode and its thickness determines both the mass transport and activation overpotential. Hence, such a systematic evaluation of these oxygen permeability characteristics in this new class of membranes designed for elevated temperature operation is essential for designing improved PEM fuel cells.

## 4. Conclusions

Electrode kinetics and mass-transport parameters were determined for perfluorinated membrane Nafion® 117 and two sulfonated poly(arylene ether sulfone) membranes SPES-40 and SPES-PS using slow sweep voltammetry and chronoamperometry at 3 atm $O_2$ pressure (total pressure) in a temperature range of 303–353 K and at 323 K temperature in a pressure range of 1–4 atm (total pressure).

Like Nafion® 117, Tafel plots for oxygen reduction at Pt|SPES-40 and SPES-PS membrane interfaces displayed two slopes corresponding to oxide covered and free Pt surface (low and high current density regions). The electrode kinetic parameters of all the membranes were found to be roughly in the same range as Nafion® 117.

The temperature dependence of $O_2$ transport parameters showed similar trends for all the membranes investigated: the $O_2$ diffusion coefficient $D$ increased with temperature, while the solubility $C$ decreased. The overall permeability $DC$ showed an increase as a function of temperature. All the SPES membranes were found to have relatively lower diffusion coefficients as compared to Nafion® 117 despite the higher water uptake (approximately twice the IEC). These results are discussed in the context of water content and microstructure of the membranes. The conformations of water-filled channels connecting the hydrophilic ionic clusters appear to have important contributions in the process of $O_2$ diffusion. The chemistry of the SPES membrane backbone appears to play a major role in determining the solubility of oxygen in these aromatic chain backbone polymer systems given its relatively lower hydrophobicity as compared to the perfluorinated backbone for Nafion®.

The pressure dependence of oxygen solubility shows an increasing trend for all the membranes as expected according to Henry's law. The diffusion coefficient of Nafion® 117 tended to be independent of pressure in the 2–4 atm region, although an initial rapid increase of $D$ with pressure was observed below 2 atm. For the two SPES membranes, an approximately linear increase of diffusion coefficient with pressure was observed. Changes in the microstructure of the membranes as a result of pressurization were proposed to be responsible for the variation of the diffusion coefficient with pressure. For all three membranes, the $O_2$ permeability increases linearly with pressure. Nafion® 117 has higher permeability than SPES-PS and SPES-40 at 323 K over the pressure range 1–4 atm (total pressure). These findings are expected to have an important effect in the application of these new alternative proton exchange membranes for elevated temperature PEM fuel cells.

## Acknowledgements

The authors wish to acknowledge financial support from the Department of Energy, through a subcontract from Los Alamos National Laboratory. The authors would like to express their deep appreciation to Professor James McGrath at the Department of Chemistry, Virginia Polytechnic Institute and State University

(Virginia Tech.) and Dr. David Ofer at Foster-Mill, Inc. (Boston, MA) for providing the proton exchange membranes used in this work. The assistance of our group members in the design and set up of the electrochemical cell as well as the humidification control unit is deeply appreciated.

## References

[1] O. Savadogo, J. New, Mater. Electrochem. Syst. 1 (1998) 47.
[2] T.A. Zawodzinski Jr., T.E. Springer, F. Uribe, S. Gottesfeld, Solid State Ionics 60 (1993) 199.
[3] F. Opekar, D. Svozil, J. Electroanal. Chem. 385 (1995) 269.
[4] Y. Sone, P. Ekdunge, D. Simonsson, J. Electrochem. Soc. 143 (1996) 1254.
[5] J.J. Sumner, S.E. Creager, J.J.A. Ma, D.D. Desmarteau, J. Electrochem. Soc. 145 (1998) 1076.
[6] P.S. Kauranen, E. Skou, J. Appl. Electrochem. 26 (1996) 909.
[7] N. Jia, M.C. Lefebvre, J. Halfyard, Z. Qi, P.G. Pickup, Electrochem. Solid-State Lett. 3 (2000) 529.
[8] S.R. Samms, S. Wasmus, R.F. Savinell, J. Electrochem. Soc. 143 (1996) 1498.
[9] K.D. Kreuer, Solid State Ionics 97 (1997) 1.
[10] S. Malhotra, R. Datta, J. Electrochem. Soc. 144 (1997) L23.
[11] R.W. Kopitzke, C.A. Linkous, G.L. Nelson, Polym. Degrad. Stab. 67 (2000) 335.
[12] S.D. Mikhailenko, S.M.J. Zaidi, S. Kaliaguine, Catal. Today 67 (2001) 225.
[13] S. Faure, N. Cornet, G. Gebel, R. Mercier, M. Pineri,B. Sillion, New Materials for Fuel Cell and Modern Battery Systems II, Proceedings of the International Symposium on New Materials for Fuel Cell and Modern Battery Systems, 2nd, Montreal, July 6–10, 1997 (1997) 818–827.
[14] R.W. Kopitzke, B.D. Seurer, T.T. Steckler, Abstracts of Papers, 223rd ACS National Meeting, Orlando, FL, United States, April 7–11, 2002 (2002) CHED-972.
[15] F. Wang, M. Hickner, Q. Ji, W. Harrison, J. Mecham, T.A. Zawodzinski, J.E. McGrath, Macromol. Symp. 175 (2001) 387.
[16] F. Lufrano, G. Squadrito, A. Patti, E. Passalacqua, J. Appl. Polym. Sci. 77 (2000) 1250.
[17] F. Lufrano, I. Gatto, P. Staiti, V. Antonucci, E. Passalacqua, Solid State Ionics 145 (2001) 47.
[18] R.W. Kopitzke, C.A. Linkous, H.R. Anderson, G.L. Nelson, J. Electrochem. Soc. 147 (2000) 1677.
[19] H.R. Allcock, M.A. Hofmann, C.M. Ambler, S.N. Lvov, X.Y. Zhou, E. Chalkova, J. Weston, J. Membr. Sci. 201 (2002) 47.
[20] M. Kawahara, M. Rikukawa, K. Sanui, N. Ogata, Solid State Ionics 136–137 (2000) 1193.
[21] M. Kawahara, M. Rikukawa, K. Sanui, Polym. Adv. Technol. 11 (2000) 544.
[22] J.M. Bae, I. Honma, M. Murata, T. Yamamoto, M. Rikukawa, N. Ogata, Solid State Ionics 147 (2002) 189.
[23] K. Miyatake, H. Iyotani, K. Yamamoto, E. Tsuchida, Macromolecules 29 (1996) 6969.
[24] R. Nolte, K. Ledjeff, M. Bauer, R. Muelhaupt, BHR Group Conf. Ser. Publ. 3 (1993) 381.
[25] R. Nolte, K. Ledjeff, M. Bauer, R. Muelhaupt, J. Membr. Sci. 83 (1993) 211.
[26] Y.S. Kim, F. Wang, M. Hickner, J.E. McGrath, T.A. Zawodzinski, Abstracts of Papers, 223rd ACS National Meeting, Orlando, FL, United States, April 7–11, 2002 (2002) POLY-015.
[27] S.R. Brankovic, J.X. Wang, R.R. Adzic, Electrochem. Solid-State Lett. 4 (2001) A217.
[28] M.A. Hickner, F. Wang, Y.S. Kim, B. Pivovar, T.A. Zawodzinski, S. McGrath, Preprints of Symposia - American Chemical Society, Division of Fuel Chemistry 46 (2001) 459-460.
[29] R.E. Kesting, Synthetic Polymeric Membranes. A Structural Perspective, second ed., Wiley, New York, 1985.
[30] M.R. Pereira, J. Yarwood, J. Chem. Soc. Faraday Trans. 92 (1996) 2731.
[31] R.M. Formato, P. Osenar, R.F. Kovar, N. Langrau, in PCT Int. Appl., Foster-Miller, Inc, USA Wo, 2000, p. 53.
[32] F. Wang, M. Hickner, Y.S. Kim, T.A. Zawodzinski, J.E. McGrath, J. Membr. Sci. 197 (2002) 231.
[33] A. Parthasarathy, C.R. Martin, S. Srinivasan, J. Electrochem. Soc. 138 (1991) 916.
[34] A. Parthasarathy, S. Srinivasan, A.J. Appleby, J. Electrochem. Soc. 139 (1992) 2530.
[35] A. Parthasarathy, S. Srinivasan, A.J. Appleby, C.R. Martin, J. Electrochem. Soc. 139 (1992) 2856.
[36] P.D. Beattie, V.I. Basura, S. Holdcroft, J. Electroanal. Chem. 468 (1999) 180.
[37] F.N. Buechi, M. Wakizoe, S. Srinivasan, J. Electrochem. Soc. 143 (1996) 927.
[38] V.I. Basura, P.D. Beattie, S. Holdcroft, J. Electroanal. Chem. 458 (1998) 1.
[39] V.I. Basura, C. Chuy, P.D. Beattie, S. Holdcroft, J. Electroanal. Chem. 501 (2001) 77.
[40] L. Zhang, C. Ma, S. Mukerjee, Electrochim. Acta 48 (2003) 1845.
[41] E.J. Stoler, B.R. Nair, R.F. Kovar, D. Ofer, in: Proceedings of the 36th Intersociety Energy Conversion Engineering Conference, 2001, pp. 975–980.
[42] J.M.D. Rodriguez, J.A.H. Melian, J.P. Pena, J. Chem. Edu. 77 (2000) 1195.
[43] T. Biegler, D.A.J. Rand, R. Woods, J. Electroanal. Chem. 29 (1971) 269.
[44] F.A. Uribe, T.E. Springer, S. Gottesfeld, J. Electrochem. Soc. 139 (1992) 765.
[45] J. Giner, J. Electrochem. Soc. 111 (1964) 376.
[46] A. Damjanovic, V. Brusic, Electrochim. Acta 12 (1967) 615.
[47] A. Damjanovic, M.A. Genshaw, Electrochim. Acta 15 (1970) 1281.
[48] J.O.'M. Bockris, A.A. Gochev, J. Electroanal. Chem. 214 (1986) 655.
[49] D.B. Sepa, M.V. Vojnovic, L.M. Vracar, A. Damjanovic, Electrochim. Acta 29 (1984) 1169.
[50] D.R. Lide, CRC Handbook of Chemistry and Physics, CRC Press, Boca Raton, Ann Arbor, London, Tokyo, 1994–1995, pp. 6–15.
[51] K.J. Laidler, J.H. Meiser, B.C. Sanctuary, Physical Chemistry, Houghton Mifflin Company, Boston, New York, 2003, p. 198.
[52] K.J. Vetter, Electrochemical Kinetics – Theoretical and Experimental Aspects, Academic Press, New York, 1967.
[53] J.T. Hinatsu, M. Mizuhata, H. Takenaka, J. Electrochem. Soc. 141 (1994) 1493.
[54] T.D. Gierke, G.E. Munn, F.C. Wilson, J. Polym. Sci. 19 (1981) 1687.
[55] W.Y. Hsu, T.D. Gierke, Macromolecules 15 (1982) 101.
[56] W.Y. Hsu, T.D. Gierke, J. Membr. Sci. 13 (1983) 307.
[57] P.J. Brookman, J.W. Nicholson, in: A.D. Wilson, H.J. Prosser (Eds.), Developments in Ionic Polymers, vol. 2, Elsevier Applied Science Publishers, London, 1986, pp. 269–283.
[58] H.J. Yeager, A. Eisenberg, Perfluorinated Ionomer Membranes, ACS Symp. Ser. 180, American Chemical Society, Washington DC, vols. 1–6, 1982, pp. 41–63.
[59] P.C. Lee, M.A.J. Rodgers, J. Phys. Chem. 88 (1984) 4385.
[60] S.J. Paddison, T.A. Zawodzinski Jr., Solid State Ionics 113–115 (1998) 333.

[61] Z. Ogumi, Z. Takehara, S. Yoshizawa, J. Electrochem. Soc. 131 (1984) 769.
[62] K.D. Kreuer, J. Membr. Sci. 185 (2001) 29.
[63] J.M. Serpico, S.G. Ehrenberg, J.J. Fontanella, X. Jiao, D. Perahia, K.A. McGrady, E.H. Sanders, G.E. Kellogg, G.E. Wnek, Macromolecules 35 (2002) 5916.
[64] Y.S. Kim, F. Wang, M. Hickner, T.A. Zawodzinski, J.E. McGrath, Polymer Preprints (American Chemical Society, Division of Polymer Chemistry) 43 (2002) 342–343.
[65] Y.S. Kim, L. Dong, M.A. Hickner, B.S. Pivovar, J.E. McGrath, Polymer 44 (2003) 5729.
[66] D. Raucher, M.D. Sefcik, ACS Symp. Ser. 223 (1983) 89–110.
[67] D. Raucher, M.D. Sefcik, Polymer Preprints (American Chemical Society, Division of Polymer Chemistry) 24 (1983) 87–88.
[68] D. Raucher, M.D. Sefcik, ACS Symp. Ser. 223 (1983) 111–124.
[69] M.D. Sefcik, J. Schaefer, F.L. May, D. Raucher, S.M. Dub, J. Polym. Sci. Polym. Phys. 21 (1983) 1041.